Molecular Biology of the Cell
Vol. 17, 4420–4434, October 2006

γ-Tubulin Is Required for Proper Recruitment and Assembly of Kar9–Bim1 Complexes in Budding Yeast[V]

Lara Cuschieri,* Rita Miller,† and Jackie Vogel*

*Department of Biology, McGill University, Montreal, Quebec, Canada H3A 1B1; and
†Department of Biology, University of Rochester, Rochester, NY 14627

Submitted March 28, 2006; Revised July 27, 2006; Accepted July 31, 2006
Monitoring Editor: Kerry Bloom

Microtubule plus-end–interacting proteins (+TIPs) promote the dynamic interactions between the plus ends (+ends) of astral microtubules and cortical actin that are required for preanaphase spindle positioning. Paradoxically, +TIPs such as the EB1 orthologue Bim1 and Kar9 also associate with spindle pole bodies (SPBs), the centrosome equivalent in budding yeast. Here, we show that deletion of four C-terminal residues of the budding yeast γ-tubulin Tub4 (*tub4-Δdsyl*) perturbs Bim1 and Kar9 localization to SPBs and Kar9-dependant spindle positioning. Surprisingly, we find Kar9 localizes to microtubule +ends in *tub4-Δdsyl* cells, but these microtubules fail to position the spindle when targeted to the bud. Using cofluorescence and coaffinity purification, we show Kar9 complexes in *tub4-Δdsyl* cells contain reduced levels of Bim1. Astral microtubule dynamics is suppressed in *tub4-Δdsyl* cells, but it are restored by deletion of Kar9. Moreover, Myo2- and F-actin–dependent dwelling of Kar9 in the bud is observed in *tub4-Δdsyl* cells, suggesting defective Kar9 complexes tether microtubule +ends to the cortex. Overproduction of Bim1, but not Kar9, restores Kar9-dependent spindle positioning in the *tub4-Δdsyl* mutant, reduces cortical dwelling, and promotes Bim1–Kar9 interactions. We propose that SPBs, via the tail of Tub4, promote the assembly of functional +TIP complexes before their deployment to microtubule +ends.

INTRODUCTION

In budding yeast, the EB1 homologue Bim1 and APC-like protein Kar9 are microtubule plus-end (+end)–interacting proteins (+TIP) that link astral microtubules to the cortex and facilitate spindle placement at the bud neck before anaphase (Carminati and Stearns, 1997; Tirnauer *et al*., 1999; Beach *et al*., 2000; Lee *et al*., 2000; Miller *et al*., 2000; Yin *et al*., 2000; Liakopoulos *et al*., 2003; Maekawa *et al*., 2003). Paradoxically, EB1/Bim1 and APC/Kar9 can also localize to microtubule-organizing centers; centrosomes or spindle pole bodies (SPBs) in yeast, independently of astral microtubules (Liakopoulos *et al*., 2003; Louie *et al*., 2004; Maekawa and Schiebel, 2004). The asymmetric localization of Kar9 to the SPB destined to enter the bud ("old" SPB, or SPB_b) and to astral microtubules that emanate from the SPB_b is critical for proper spindle placement and orientation (Liakopoulos *et al*., 2003; Maekawa *et al*., 2003; Maekawa and Schiebel, 2004; Moore *et al*., 2006). However, any functional significance between the SPB localization of +TIP proteins and their subsequent function on astral microtubule +ends has not been clearly demonstrated. It has been proposed that SPB components may promote the assembly of +TIP complexes at the SPB before their deployment onto the microtubule (Liakopoulos *et al*., 2003). Thus, mutations in SPB components that perturb the localization of Bim1 and/or Kar9 at SPBs, but do not block the assembly of astral microtubules, may reveal additional functional significance of their initial localization to these organelles.

γ-Tubulin (Tub4) localizes to SPBs and initiates microtubule nucleation solely from these organelles in budding yeast (Sobel and Snyder, 1995; Marschall *et al*., 1996; Spang *et al*., 1996). Significantly, mutations in the carboxy-terminal (C-terminal) tail of Tub4 do not perturb the assembly of astral microtubules but instead affect their organization (Vogel and Snyder, 2000; Vogel *et al*., 2001). In particular, an internal deletion of the DSYLD residues of the acidic C-terminal tail of Tub4 (*tub4-Δdsyld*) was previously shown to promote the formation of stable astral microtubules that terminated in the cortex of the bud (Vogel and Snyder, 2000). In addition, preanaphase spindles in *tub4-Δdsyld* cells were frequently found displaced from the bud neck and associated with stabilized astral microtubules that terminated at the bud cortex (Vogel and Snyder, 2000). The effect of the *tub4-Δdsyld* mutation on astral microtubule organization was specific to astral microtubules that enter the bud, suggesting the cortex may play a role in the formation of these stable arrays. Consistent with this possibility, astral microtubules that projected to the bud cortex persisted in the presence of microtubule-destabilizing drugs, whereas astral microtubules that projected into the mother were depolymerized (Vogel and Snyder, 2000). These observations, in combination with the previously described SPB localization of Kar9 and Bim1 (Liakopoulos *et al*., 2003; Maekawa *et al*., 2003; Maekawa and Schiebel, 2004), led us to investigate whether Tub4 might be important for the localization of Kar9 and Bim1 to SPBs and ultimately for their function on the +ends of astral microtubules during spindle positioning. Moreover, we speculated that the DSYL residues, which lie in the highly unstructured and acidic tail of γ-tubulin (Aldaz

This article was published online ahead of print in *MBC in Press* (http://www.molbiolcell.org/cgi/doi/10.1091/mbc.E06–03–0245) on August 9, 2006.

[V] The online version of this article contains supplemental material at *MBC Online* (http://www.molbiolcell.org).

Address correspondence to: Jackie Vogel (jackie.vogel@mcgill.ca).

Abbreviations used: +end, microtubule plus end; +TIP, plus tip protein; SPB, spindle pole body.

et al., 2005), might be important for this aspect of Tub4 function.

In this study, we show that the localization of Bim1 and Kar9 to SPBs is defective in *tub4-Δdsyl* cells and that the *tub4-Δdsyl* mutation perturbs the function of the Kar9 pathway for spindle positioning. We demonstrate that defects in spindle positioning are not due to failure of Kar9 to localize to +ends, but rather they are due to defective Kar9 complexes that are localized to astral microtubules that enter the bud but ultimately fail to position the spindle at the bud neck. These Kar9 complexes seem to stabilize the +ends of astral microtubules terminating in the bud, resulting in long astral microtubules and increased dwell time of Kar9 at the bud cortex. Finally, we show that overproduction of Bim1 but not Kar9 restores Bim1–Kar9 physical interactions, efficient delivery of microtubules into the bud and spindle placement, and dynamic interactions between Kar9-loaded microtubule +ends and the bud cortex in *tub4-Δdsyl* cells. Our analysis suggests that the DSYL residues of the Tub4 C terminus are important for the proper loading and/or assembly of functional Bim1–Kar9 complexes at SPBs before their deployment to astral microtubules.

MATERIALS AND METHODS

Strain Construction and Plasmids

Strains were created through polymerase chain reaction (PCR)-based transformation, standard nonintegrative plasmid transformation and mating procedures as described previously (Christianson *et al*., 1992; Longtine *et al*., 1998). Media (rich media, YPAD; and synthetic complete, SC) and general yeast methods are as described previously (Guthrie and Fink, 1991). The *tub4-Δdsyl* mutation removes the N-terminal Asp and hydrophobic SYL residues of the previously described DSYLD domain (Vogel and Snyder, 2000). Homologous recombination was used to replace the *TUB4* open reading frame with the *tub4-Δdsyl* allele as described previously for *tub4-Y445D* (Vogel *et al*., 2001).

Genetic (Synthetic Lethality) Analysis

For synthetic lethality analysis, heterozygous diploid strains were sporulated in low nitrogen liquid medium, and meiotic products (tetrads) were obtained (Guthrie and Fink, 1991). Tetrads were dissected on a Nikon E400 micromanipulator. For each analysis, meiotic products of 40 tetrads (spores) were grown on YPAD medium at 25°C, and the segregation of alleles was determined by replating spores on appropriate selection media at permissive (25°C) and restrictive (30 and 37°C) temperatures. The segregation of *tub4* alleles was confirmed by growth on minimal medium lacking tryptophane and by suppression of growth on rich medium at 37°C as described previously (Vogel *et al*., 2001). The segregation of array mutations (*geneΔ::KanMX*) was confirmed on YPAD containing 200 μg/ml G418 (Geneticin; Invitrogen, Burlington, Ontario, Canada).

Statistical Analysis

Data from three independent experiments were used for measuring astral microtubule dynamics and quantitative analysis of fluorescence intensity. The average value for each analysis was determined, and the SE of the mean was calculated (y-error bars, representing the precision of the measurement) using Excel (Microsoft, Redmond, WA). Where indicated, significance (defined as a $p < 0.01$) was determined using the SD of the samples (population) for a two-tailed homoscedastic Student's *t* test. All calculations were performed with Excel.

Fluorescent Microscopy Methods

For time-lapse imaging, overnight cultures were grown in either YPAD or fluorescent protein (FP) medium (Pot *et al*., 2005) at the permissive temperature of 25°C, diluted to a cell density of ~0.1 OD units ml^{-1} and then regrown to a density of ~0.4 OD units ml^{-1}. Yeast cells were collected by centrifugation, washed twice with fresh FP medium, and mounted on 2% agarose/FPM pads sealed with Valap (petroleum jelly:lanolin:paraffin [1:1:1]). All microscopic analysis was performed at 25°C unless otherwise indicated. For analysis of microtubule guidance, live cells were examined using a deconvolution imaging system mounted on a Nikon TE2000-U (Pot *et al*., 2005). Optical sections were acquired at 0.5-μm intervals in 6.0-μm stack using Openlab Automator Pro (Improvision UK, Coventry, United Kingdom).

Single-channel imaging of astral microtubule dynamics (GFP–Tub1) and multichannel four-dimensional imaging of Spc42-red fluorescent protein (RFP), cyan fluorescent protein (CFP)–Tub1, Bim1–CFP, Bim1–green fluorescent protein (GFP), Kar9–GFP, and Kar9–yellow fluorescent protein (YFP) fluorescent fusion proteins was performed using a WaveFX spinning disk confocal system (Quorum Technologies, Guelph, Ontario, Canada) mounted on a Leica DM 5000 upright motorized microscope equipped with a Synapse Diode Laser merge module (Quorum Technologies) with lines for 440 nm (14-mW coupled output) and 491 nm (13-mW coupled output) excitation, a modified Yokagawa CSU10 Nipkow Disk scan head, and a Hamamatsu C9100-12 back thinned electronmultiplying charge-coupled device camera. An Exfo light source and appropriate excitation and emission filters were used for detection of RFP. Optical sections (0.5 or 0.75 μm) were acquired through a 4.0-μm stack, either continuously or at 5-s intervals by using Volocity 3DM (Improvision UK). For microtubule dynamics, optical sections (0.3 μm) were acquired through a 4.0-μm stack at 10-s intervals for a total time of 5 min.

Calculation of Microtubule Dynamics

Microtubule dynamics (elongation rates, shrinkage rates, and pauses) were determined by measuring microtubule lifetime lengths by using Volocity 3DM (Improvision UK). Microtubule lengths were measured in triplicate, and the average value for each time point were used for calculations. Elongation were defined as three consecutive points on a regression line in which the increased change in length of a microtubule ($\Delta length_{increase}$) was ≥0.3 μm. Shrinkage was defined as three consecutive points on a regression line in which the decreased change in length of a microtubule ($\Delta length_{decrease}$) was ≥0.3 μm. Microtubule pausing was defined as a change in length spanning three points on a regression line that was ≤0.3 μm. Microtubule catastrophes were defined as shrinkage after growth or pause, whereas microtubule rescues were defined as transitions to growth after a shrinkage or pause (Adames and Cooper, 2000). The frequencies of catastrophe and rescue were calculated as described previously (Kosco *et al*., 2001).

Kar9–GFP +End Tracking Method

Dynamic movement of Kar9–GFP on microtubule +ends was tracked using Volocity Classification module (Improvision UK). To track Kar9–GFP movements in the conditional *myo2-16* allele, cells were grown in rich medium at a restrictive temperature for *myo2-16* (Schott *et al*., 1999) that is not restrictive for the *tub4-Δdsyl* allele (30°C). A Kar9 classifier (a representative 3-dimensional volume for a given fluorophore) was created based on the shape and size defined by Kar9–GFP associated with astral microtubules in wild-type cells. This classifier was used to track Kar9–GFP on +ends in space and time for representative small-budded cells of each strain from three independent experiments. The classifier was defined to automatically join broken tracks and fill empty holes of fluorescence. In addition, the classifier was restricted to track Kar9–GFP between an average minimum and maximum fluorescent intensity per cell. In time points where the Kar9–GFP intensity either exceeded or failed to meet the intensity requirements of the classifier, manual tracking was used. Finally, tracks were confirmed manually using frames from the original image sequence.

Quantitative Fluorescence

For quantitative fluorescence measurements, image stacks were acquired with a WaveFX confocal system by using the following exposures: Kar9–GFP (300 ms), Kar9–YFP (colocalization experiments, 500 ms), and Bim1–CFP (100 ms). Image series were deconvolved to 90% confidence or 25 iterations by using the Volocity Restoration module (Improvision UK). For each analysis, fluorescence intensities were measured in >100 cells per strain and/or condition in three independent experiments. An 8.0 voxel volume was used for each measurement. Background signal was calculated as the averaged intensity of four equivalent volumes located inside of the cell. Fluorescent intensities (average/volume for the deconvolved image) were calculated using the Volocity Visualization module (Improvision) and background subtracted, resulting in corrected fluorescence units (FU).

Protein Methods and Coimmunoprecipitation

All steps were performed at 4°C unless indicated otherwise. Whole cell extracts were prepared as described previously (Vogel *et al*., 2001). Extracts were clarified by centrifugation for 10 min at 14,000 × *g*. For immunoprecipitations (IPs), 900 μl of 1× IP buffer (lysis buffer + 0.1% NP-40) was added to clarified extracts. An aliquot of undiluted extract (input) was diluted 1:1 with 2× sample buffer (SB) for analysis. Diluted extracts were incubated with pre-equilibrated IgG-Sepharose (25 μl; 50% slurry) for 2 h. Beads were washed six times with IP buffer, pelleted at 2000 × *g* for 1 min, and the supernatant was aspirated. Bound proteins were recovered from the beads by incubating in 25 μl of 2× SB for 7 min at 90°C.

Electrophoresis and Immunoblotting

SDS-PAGE and immunoblotting were performed as described previously (Vogel *et al*., 2001). Anti-TAP (ProA detection; Open Biosystems, Huntsville AL) was used at 1:7000 in Tris-buffered saline/0.20% Tween 20 (TBS-T). A polyclonal anti-Bim1 antibody was used at 1:4000. Monoclonal anti-actin (MP

Biomedicals, Irvine, CA) was used at 1:5000 in TBS-T. Anti-rabbit (anti-TAP and anti-Bim1) or mouse (anti-actin) horseradish peroxidase-conjugated secondary antibodies were used at 1:10,000 in TBS-T (GE Healthcare, Little Chalfont, Buckinghamshire, United Kingdom). Protein/antibody complexes were detected using enhanced chemiluminescence (GE Healthcare).

Latrunculin B (LatB), Phalloidin, and Nocodazole (NZ) Treatment

Cells were grown overnight in FP medium, diluted to a cell density of ~0.1 OD units ml^{-1}, and then regrown to a density of ~0.4 OD units ml^{-1}. Cells were incubated in FP medium containing 200 μM LatB (Sigma-Aldrich, St. Louis, MO) for 30–60 min at 25°C to depolymerize actin structures. Disruption of F-actin in LatB-treated cells was confirmed by staining an aliquot of fixed, treated cells with Alexa 488-phalloidin (Molecular Probes/Invitrogen). To depolymerize microtubules, cells were incubated in FP medium containing 30 μg/ml NZ for 30 min at 18°C. Disruption of astral microtubules and spindle collapse was confirmed by imaging CFP–tubulin-labeled microtubules.

RESULTS

Localization of Bim1 and Kar9 to SPBs Is Defective in tub4-Δdsyl Cells

Bim1 and Kar9 localize to SPBs independently of their association with microtubules in small-budded cells with high levels of the early B-type Cyclins Clb3 and Clb4 (Liakopoulos *et al*., 2003). Although Kar9 localization to SPBs is partially dependant on Bim1 (Miller *et al*., 2000; Liakopoulos *et al*., 2003), the SPB scaffold for Kar9 loading has not yet been fully characterized. Tub4 has been shown to localize exclusively to SPBs in budding yeast (Sobel and Snyder, 1995; Marschall *et al*., 1996). However *tub4-Y445D* and *tub4-Δdsyld* cells exhibit defects in microtubule organization and altered microtubule dynamics (Vogel and Snyder, 2000; Vogel *et al*., 2001), suggesting that proteins associated specifically with the minus end (−end) of microtubules can influence the behavior of the microtubule +end. We first confirmed the exclusive localization of Tub4 to SPBs by analysis of the colocalization of a functional Tub4–CFP fusion protein with Spc42–RFP (SPBs) and Bim1–GFP (+ends); although Tub4–CFP fluorescence was detected at SPBs, no signal above background was detected at +ends (our unpublished data). We therefore asked whether these *tub4* mutants might exert their effect on microtubule +ends by influencing the localization of Bim1 and/or Kar9 to SPBs. We reasoned that if these mutants reduced Bim1 and/or Kar9 recruitment to or interaction at SPBs, these proteins would be defective in their localization to SPBs in the absence of microtubules. To test this hypothesis, wild-type, *tub4-Y455D*, and *tub4-Δdsyl* cells expressing Bim1–GFP and CFP–Tub1 were treated with the microtubule-destabilizing drug NZ (30 μg/ml), and small-budded cells were scored for Bim1–GFP colocalization to the collapsed spindle (seen as single focus of CFP–tubulin). Bim1–GFP localized to the collapsed spindle in the majority of wild-type (82%; n = 141 cells) and *tub4-Y445D* cells (77%; n = 119) lacking astral microtubules (Figure 1, A and B). However, Bim1–GFP was rarely detected in *tub4-Δdsyl* cells (24%; n = 115 cells) lacking astral microtubules (Figure 1, A and B).

To determine whether the localization of Kar9–GFP to the SPB_b was similarly defective in *tub4-Δdsyl* cells, wild-type, *tub4-Y445D*, and *tub4-Δdsyl* cells expressing Kar9–GFP, CFP–Tub1, and the SPBb-specific marker Spc42–RFP (Pereira *et al*., 2001) were treated with 30 μg/ml NZ and assessed for colocalization of Kar9–GFP with Spc42–RFP. NZ treatment depolymerized the astral microtubules and collapsed bipolar spindles to a single focus of CFP–Tub1 in wild-type, *tub4-Y445D*, and *tub4-Δdsyl* cells coexpressing Kar9–GFP (Figure 1C). Kar9–GFP colocalized with Spc42–RFP in the majority of wild-type (84%; n = 90 cells) and *tub4–Y445D* (78%; n = 116 cells) cells lacking astral microtubules (Figure 1, C and D). Similar to Bim1, Kar9–GFP was rarely detected at the SPB in *tub4-Δdsyl* cells lacking astral microtubules (24%; n = 85 cells; Figure 1, C and D). This analysis suggested the localization of Bim1 and Kar9 to SPBs is defective in *tub4-Δdsyl* cells and that the DSYL residues influence the association of these proteins with SPBs.

DSYL Residues Are Required for Proper Function of the Kar9 Pathway

The defect in SPB localization of Bim1 and Kar9 in the *tub4-Δdsyl* mutant suggested that loss of the DSYL residues might perturb the Kar9 pathway for spindle positioning Genes acting in dynein-dependent spindle positioning (*DHC1*, *KIP2*, and *ARP1;* Figure 2A) are essential for life when the Kar9 pathway is disrupted (Miller and Rose, 1998). Correspondingly, mutations that disrupt Kar9 function (Figure 2A) are lethal in combination with mutations in the dynein pathway (Miller and Rose, 1998). To determine whether the *tub4-Δdsyl* mutation perturbed the function of the Kar9 pathway, we tested for synthetic lethal interactions between the *tub4-Δdsyl* mutant and mutations in genes acting in the dynein pathway. As a control, we tested for synthetic lethality with the *tub4-Y445D* mutation, which did not alter the localization of Kar9 or Bim1 to SPBs. We observed that mutations in the dynein pathway (*dhc1Δ*, *kip2Δ*, *arp1Δ*) were synthetically lethal in combination with the *tub4-Δdsyl* allele but not the *tub4-Y445D* allele (Figure 2B; representative tetrads shown in Figure 2C). Consistent with a defect in the Kar9 pathway, we found mutations in the majority of genes acting in the Kar9 pathway were not synthetically lethal with either *tub4* allele (Figure 2, B and C). One exception was a null mutation in *BIM1* (*bimΔ*). Bim1 has a complex genetic interaction network that is not restricted to Kar9 function and may include a role in chromosome segregation (Tong *et al*., 2001); consistent with this possibility, the *tub4-Δdsyl* and *tub4-Y445D* mutations were lethal in combination with deletion of the spindle checkpoint protein Mad2 (*mad2Δ*). The observed pattern of synthetic lethal interactions for the *tub4-Δdsyl* mutant indicates that the dynein pathway is essential in *tub4-Δdsyl* cells and is consistent with the hypothesis that the *tub4-Δdsyl* mutation perturbs Kar9 pathway function.

Kar9 promotes the targeting of astral microtubule +ends into the bud through its association with Myo2 and polarized actin cables, which terminate in the bud tip (Liakopoulos *et al*., 2003). We therefore tested whether the *tub4-Δdsyl* mutation would mimic the loss of function *kar9Δ* mutant and perturb targeting of astral microtubules into the bud (Figure 2D). Astral microtubule targeting was assessed in wild-type and *tub4-Δdsyl* cells expressing GFP–Tub1 (Straight *et al*., 1997). The appearance of a misguided microtubule, which emanated from the SPB proximal to the bud with its +end in the mother cell, was rare in wild-type cells (0.07 events/min, n = 300 cells) but increased fivefold in *tub4-Δdsyl* cells (0.45 events/min; n = 300 cells; $p > 0.01$; Figure 2D). This defect in targeting was consistent with a defect in the function of the Kar9 pathway. Surprisingly, we observed that the major defect in spindle positioning was displacement (>2 μm) of the spindle from the neck, rather than a failure to orient (Figure 2E). In all cases, displaced spindles (oriented either parallel or perpendicular to the long axis of the cell) were associated with a bud-directed astral microtubule that extended to the cortex. The percentage of cells containing an oriented spindle positioned near the bud neck was greater in the wild-type strain (61%; n = 300 cells) relative to the *tub4-Δdsyl* mutant (20%; n = 300 cells; Figure 2E). The percentage of cells with an unaligned spindle positioned

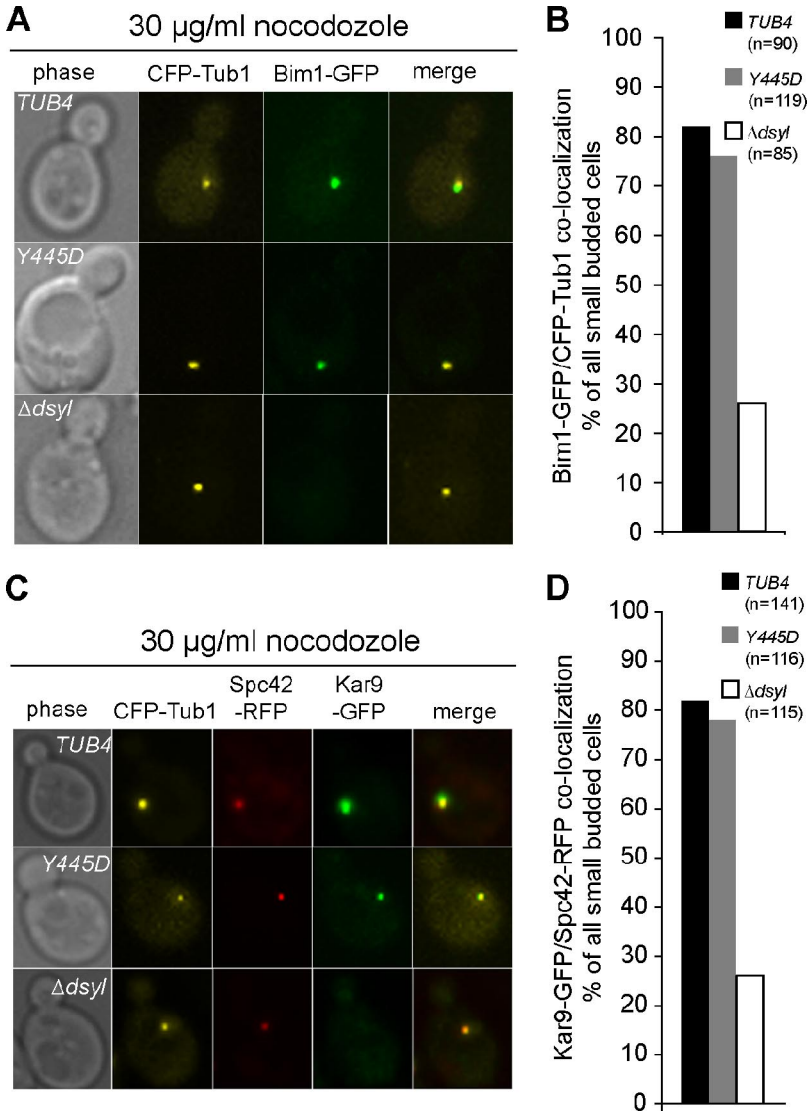

Figure 1. Localization of Bim1 and Kar9 to SPBs is defective in *tub4-Δdsyl* cells. (A) *TUB4* and *tub4-Y445D* cells treated with 30 μg/ml NZ had detectable Bim1–GFP foci associated with the collapsed spindle (single focus of CFP–Tub1), whereas the majority of *tub4-Δdsyl* cells treated with NZ did not. (B) Histogram showing the percentage of *TUB4*, *tub4-Y445D*, and *tub4-Δdsyl* cells with detectable Bim1–GFP foci at collapsed spindles after NZ treatment. (C) *TUB4* and *tub4-Y445D* cells treated with NZ had Kar9–GFP foci localized to the SPB_b. In contrast, the majority of *tub4-Δdsyl* cells lacked detectable Kar9–GFP foci associated with SPBs. Spc42–RFP marks the SPB_b. Microtubules are labeled with CFP–Tub1. (D) Histogram indicating the percentage of *TUB4*, *tub4-Y445D*, and *tub4-Δdsyl* cells exhibiting Kar9–GFP foci at SPBs.

near the bud neck (a characteristic intermediate of normal spindle positioning) was also greater in wild type (23%; n = 300 cells) relative to the *tub4-Δdsyl* mutant (15%; n = 300 cells; Figure 2E). In contrast, the percentage of cells with a bud-directed microtubule associated with a spindle positioned far from the bud neck was dramatically increased in the *tub4-Δdsyl* mutant (65%) relative to wild type (<10%; Figure 2D). This analysis suggested that the ability of bud-directed microtubules to mediate proper placement of the preanaphase spindle at the bud neck is perturbed by the *tub4-Δdsyl* mutation.

Kar9 Preferentially Localizes to Astral Microtubule +Ends in tub4-Δdsyl Cells

In wild-type cells, Kar9 localizes to the SPB_b, which is destined to enter the bud, and to the +ends of astral microtubules associated with this pole (Liakopoulos *et al.*, 2003; Maekawa *et al.*, 2003). We expected that the defect in spindle placement at the neck observed in *tub4-Δdsyl* cells resulted from a defect in the ability of Kar9 to localize to SPB_b and its associated astral microtubules. We examined the localization of Kar9–GFP in wild-type and *tub4-Δdsyl* cells coexpressing CFP–Tub1 (Figure 3A). Unexpectedly, we found that in *tub4-Δdsyl* cells, Kar9–GFP localizes to the +ends of astral microtubules (Figure 3, A and C). Quantitative fluorescence analysis suggested that the amount of Kar9–GFP associated with microtubule +ends was significantly increased in *tub4-Δdsyl* cells (658.1 ± 73.24 FU) relative to wild-type cells (396.2 ± 101.72 FU; $p < 0.01$; Figure 3B). Conversely, we found Kar9–GFP localization at the SPB was greatly reduced in *tub4-Δdsyl* cells (21.4%; n = 200 cells) relative to wild-type cells (51.5%; n = 200 cells; Figure 3, A and C). This analysis suggested that although Kar9–GFP localization to the SPB is defective in *tub4-Δdsyl* cells, Kar9 localization to microtubule +ends persists.

The majority of *tub4-Δdsyl* cells had mispositioned spindles associated with astral microtubules whose +ends terminated in the bud (Figure 2E). We therefore asked whether microtubule that entered the bud were loaded with Kar9–GFP and assessed the localization of Kar9–GFP in relation to the targeting of astral microtubules (bud versus mother) in wild-type and *tub4-Δdsyl* cells expressing CFP–Tub1 (Figure 3D). Although the percentage of cells with Kar9–GFP-loaded microtubules terminating in the mother increased in the *tub4-Δdsyl* strain (33%; n = 83 cells) relative to wild type (7%; n = 97 cells; Figure 3D), we found the majority of microtubules loaded with Kar9–GFP were appropriately

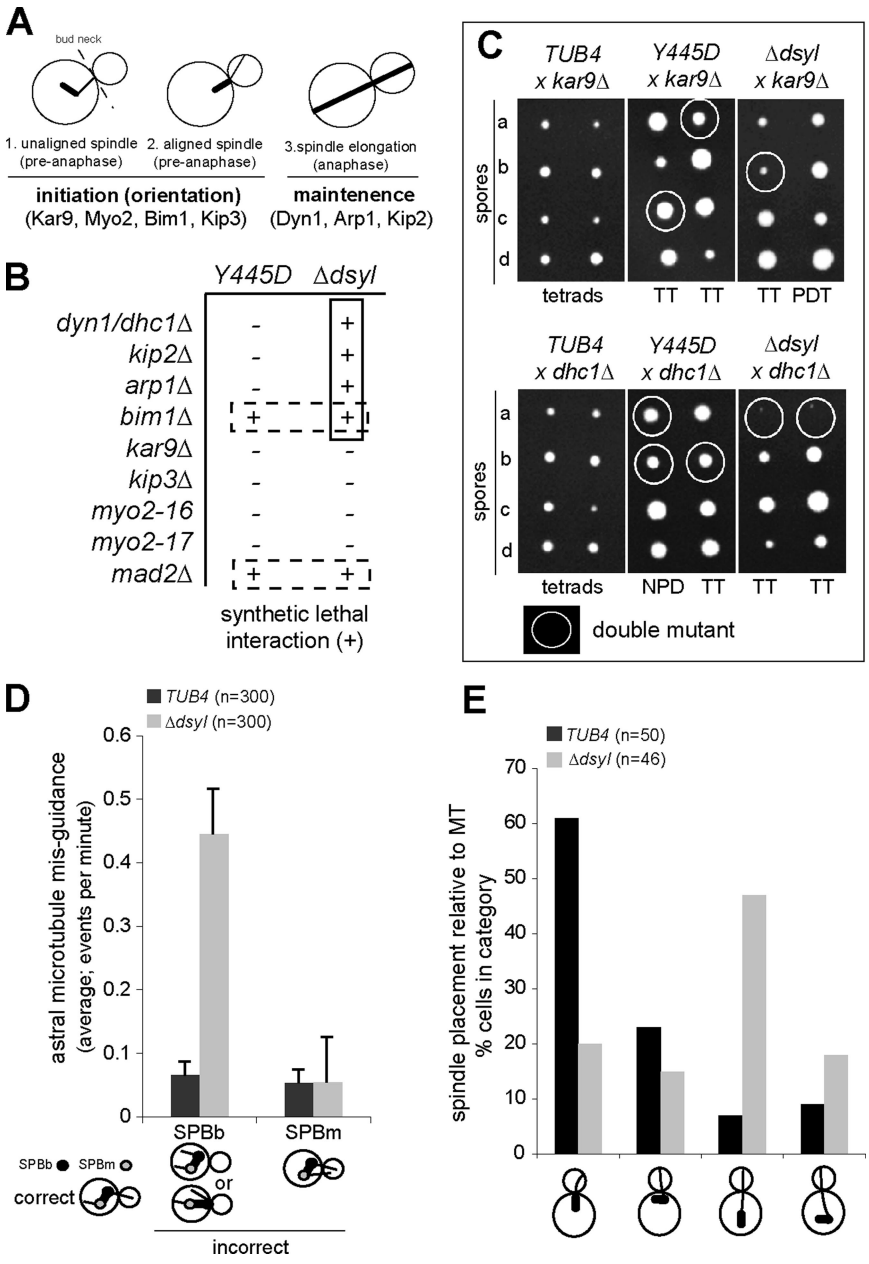

Figure 2. DSYL residues are required for function of the Kar9 pathway. (A) Cartoon of spindle positioning pathways in budding yeast. Early spindle placement is dependent on the Kar9 pathway, whereas the maintenance of spindle placement during anaphase requires the dynein pathway. (B) Query alleles (*tub4-Y445D* and *tub4-Δdsyl*) were analyzed for synthetic lethal interactions with mutations that disrupt either Kar9 or Dhc1 function. Synthetic lethal (+) and viable interactions (−) are indicated. The *tub4-Δdsyl* allele was synthetically lethal with mutations that disrupt Dhc1 function but not Kar9 function. (C) Representative tetrads for the analysis in B. Double mutant spores are circled. *tub4-Δdsyl dhc1Δ* double mutants failed to grow, whereas *tub4-Δdsyl kar9Δ* double mutants were viable. n = 40 tetrads for each cross. (D) The frequency of astral microtubule misguidance (visualized by GFP–Tub1) that occurred from the mother-bound SPB (SPB_m) or SPB_b was measured in *TUB4* and *tub4-Δdsyl* cells. *tub4-Δdsyl* cells had a higher frequency of microtubule misguidance relative to wild-type. n = 300. (E) Analysis of spindle placement in *TUB4* and *tub4-Δdsyl* cells. *tub4-Δdsyl* cells had a higher frequency of spindles that were positioned far from the bud neck relative to *TUB4* cells. n = 300. Categories of spindle placement assessed are represented in the cartoon image.

targeted to the bud (Figure 3D). We next asked whether these astral microtubules were attached to spindle at the bud neck or to a displaced spindle in the mother cell (>2 μm from the neck). In cells with a Kar9-loaded microtubule in the bud, the microtubule was attached to a displaced spindle positioned in the mother in 72.7% of *tub4-Δdsyl* cells (n = 55) but only 13.3% of wild-type cells (n = 90; Figure 3E). These findings suggested that in *tub4-Δdsyl* cells, Kar9-complexes associated with properly targeted microtubules are defective in positioning the spindle at the bud neck.

Bim1–Kar9 Stoichiometry Is Reduced in tub4-Δdsyl Cells

Bim1 is required for Kar9 localization to microtubules (Miller *et al*., 2000; Liakopoulos *et al*., 2003). Because the *tub4-Δdsyl* mutation reduced Kar9 and Bim1 localization to SPBs in the presence of NZ (Figure 1, A and C), we expected that Bim1 would similarly localize to microtubule +ends in *tub4-Δdsyl* cells. The colocalization of Bim1 and Kar9 at +ends was assessed in *TUB4* and *tub4-Δdsyl* cells expressing Bim1–CFP and Kar9–YFP (Figure 4A). Surprisingly, this analysis indicated that unlike Kar9, the amount of Bim1–CFP that localized to microtubule +ends was decreased in *tub4-Δdsyl* cells (208.5 ± 27.95 FU; $p < 0.01$) relative to wild-type cells (394.1 ± 52.73 FU; $p < 0.01$; Figure 4, A and B). Consistently, the ratio of Bim1–CFP/Kar9–GFP fluorescence intensities colocalizing on microtubule +ends was also decreased in *tub4-Δdsyl* cells (0.38 ± 0.078 FU) relative to wild-type cells (0.96 ± 0.224 FU, $p < 0.01$; Figure 4C).

Levels of Bim1 and Kar9–ProA protein were similar in whole cell extracts prepared from wild-type and *tub4-Δdsyl* cells; thus, the altered localization of these proteins was not due to their decreased stability in *tub4-Δdsyl* cells (Figure 4, D and E). Instead, this analysis suggested physical interactions between Kar9 and Bim1 might be defective in the

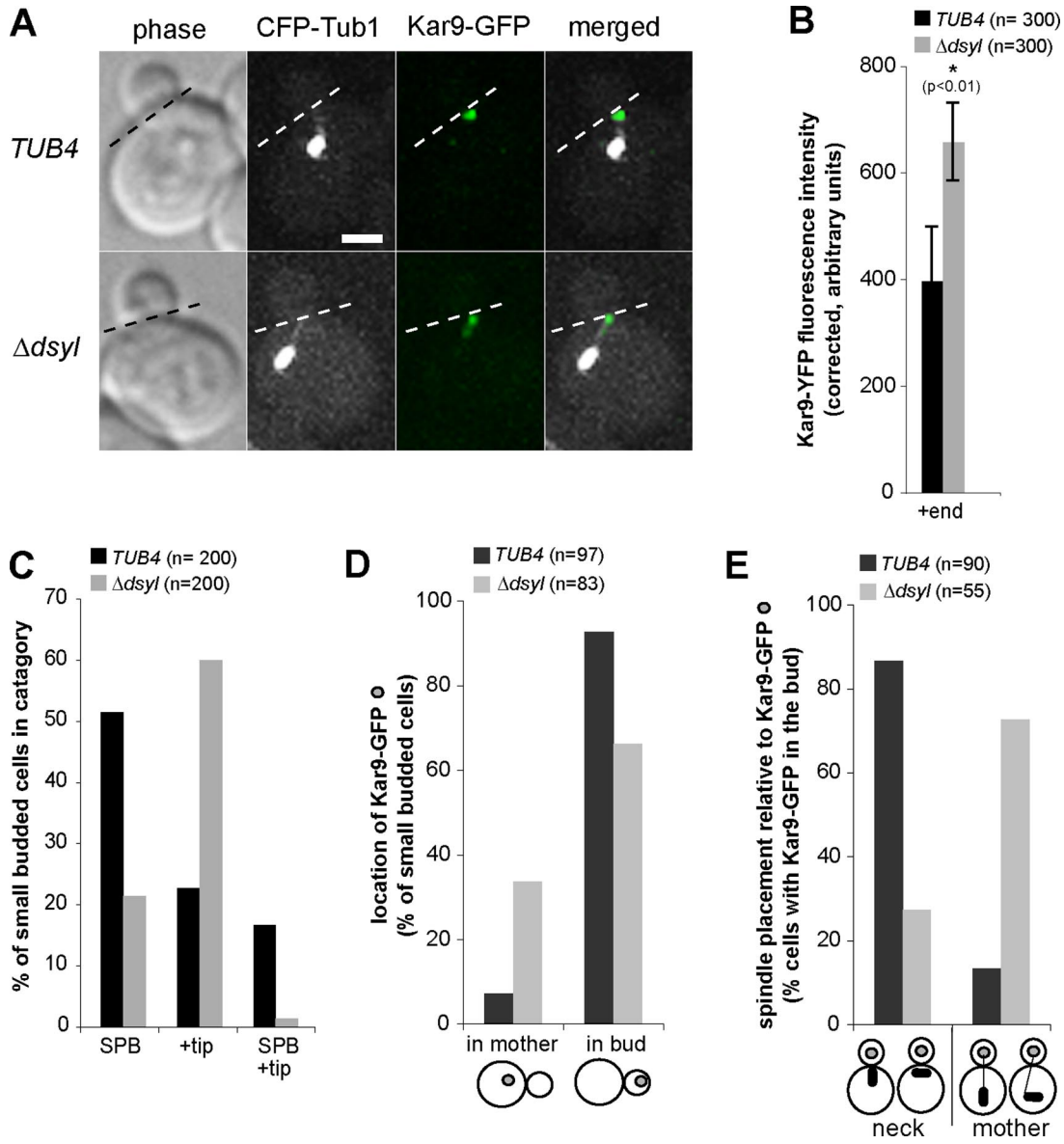

Figure 3. Kar9 preferentially localizes to astral microtubule +ends in *tub4-Δdsyl* cells. (A) In *tub4-Δdsyl* cells, Kar9–GFP localized to the +ends of astral microtubules. Dashed line indicates the position of the bud neck. Bar, 2 μm. (B) Histogram indicating the fluorescent intensities of Kar9–GFP foci associated with microtubule +ends in *TUB4* and *tub4-Δdsyl* cells. *tub4-Δdsyl* cells ($n = 300$; $p < 0.01$) have a higher average fluorescent intensity of Kar9–GFP associated with microtubule +ends relative to those of *TUB4* ($n = 300$; $p < 0.01$) cells. (C) Quantification of Kar9 localization in *TUB4* and *tub4-Δdsyl* cells. The majority of *tub4-Δdsyl* cells have Kar9–GFP foci associated with microtubule +ends. (D) Histogram indicating the localization of Kar9–GFP foci in *TUB4* and *tub4-Δdsyl* cells. The majority of Kar9–GFP foci are located within the bud for both cell types. (E) Spindle positioning relative to Kar9–GFP foci was analyzed in *TUB4* and *tub4-Δdsyl* cells. In *tub4-Δdsyl* cells, spindles remain mispositioned even when a Kar9-loaded astral microtubule is properly targeted into the bud. Categories of spindle placement assessed are represented in the cartoon image.

tub4-Δdsyl mutant. To test this possibility, the amount of Bim1 copurifying with Kar9–ProA was measured in both wild-type and *tub4-Δdsyl* cells. Kar9–ProA was isolated from whole cell extracts by IgG-Sepharose affinity purification (Puig *et al.*, 2001), and the amount of copurifying Bim1 was detected with anti-Bim1 polyclonal antibodies. This analysis revealed reduced levels of Bim1 copurifying with Kar9–ProA isolated from *tub4-Δdsyl* cells relative to wild type (Figure 4F). The amount of copurifying Bim1 (arbitrary units) normalized to the Kar9–ProA input from three independent experiments was averaged for the wild-type and *tub4-Δdsyl* strains and is shown in Figure 4G. Together, these results suggest that the ratio of Bim1 and Kar9 on microtubule +ends is decreased as a consequence of the *tub4-Δdsyl* mutation.

Kar9 Suppresses Microtubule Dynamics in tub4-Δdsyl Cells

The failure of Kar9-loaded microtubules to properly position spindles in *tub4-Δdsyl* cells may be the result of defective complexes tethering microtubule +ends to the cortex. Spindle positioning defects could also result from an alteration of the microtubule structure that suppresses the dynamic properties of microtubule +ends (e.g., a mutation in Tub4 changes the microtubule structure). To test these possibili-

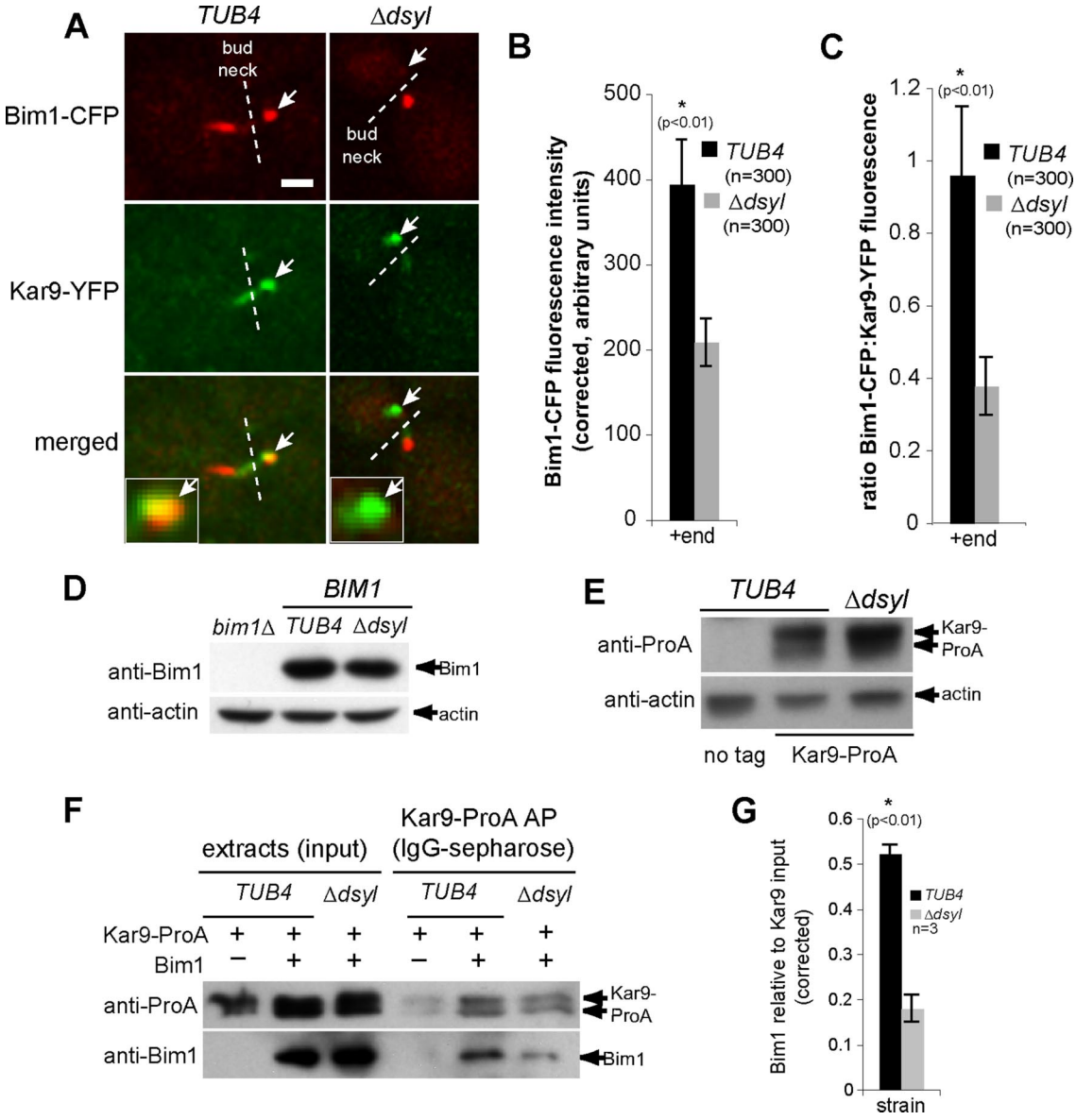

Figure 4. Stoichiometry of Bim1–Kar9 complexes is reduced in *tub4-Δdsyl* cells. (A) In *TUB4* cells, Bim1–CFP and Kar9–YFP are observed on microtubule +ends (white arrows). In contrast, Kar9–YFP foci are detected on +ends lacking detectable Bim1–CFP (white arrows) in the majority of *tub4-Δdsyl* cells. White dashed line indicates bud neck. Bar, 2 μm. (B) Quantification of Bim1–CFP fluorescence indicated that the amount of Bim1 localized to microtubule +ends is significantly reduced in *tub4-Δdsyl* cells relative to wild-type ($p < 0.01$). (C) The ratio of Bim1–CFP/Kar9–YFP fluorescence is greater in *TUB4* cells (0.958 ± 0.224 arbitrary fluorescent units) relative to *tub4-Δdsyl* cells (0.377 ± 0.078 arbitrary fluorescent units). (D and E) Bim1 and Kar9 protein levels in *tub4-Δdsyl* cells are similar to those in *TUB4* cells. Actin acts as a loading control. (F) Bim1 copurifies with Kar9–ProA in wild-type and *tub4-Δdsyl* cells, but the level of Bim1 copurification is reduced in *tub4-Δdsyl* cells. (G) Histogram showing the averaged amount of copurifying Bim1 (arbitrary units normalized to the Kar9–ProA input) in three independent experiments for wild-type and *tub4-Δdsyl* strains.

ties, we investigated the impact of Kar9 on the dynamics of astral microtubules in the bud in *TUB4*, *tub4-Δdsyl*, *kar9Δ*, and *tub4-Δdsyl kar9Δ* cells expressing GFP–Tub1. The rate of elongation and shrinkage (μm/min), frequencies (event/s) of catastrophe and rescue, and the duration of elongation, shrinkage and pauses (minutes) were calculated for astral microtubule targeted to the bud as described previously (Adames and Cooper, 2000; Kosco *et al*., 2001; for experimental details, see *Materials and Methods*). The analysis was restricted to small-budded cells. The results of this analysis are presented in Table 1, and representative microtubule lifetime length plots for each strain are shown in Figure 5.

We reasoned that if spindle positioning defects in *tub4-Δdsyl* cells resulted from an altered microtubule lattice, then microtubule dynamics would be similar in *tub4-Δdsyl* and *tub4-Δdysl kar9Δ* cells. However, if defective Kar9-complexes suppressed dynamics, deletion of Kar9 in the *tub4-Δdsyl* strain would be expected to promote dynamics. The rates of elongation and shrinkage, the frequencies and durations of catastrophes and rescues, and the duration of pauses were calculated for astral microtubules terminating in the bud in representative small-budded cells for each strain (Table 1). We found that astral microtubules in *tub4-Δdsyl* cells exhibited slightly decreased elongation rate (0.92 ± 0.19 $\mu m \cdot min^{-1}$, $p <$

Table 1. Dynamics of bud-directed astral microtubules

	Strain			
Rates (μm/min)	*TUB4*	*kar9*Δ	*tub4-*Δ*dsyl*	*kar9*Δ, *tub4-*Δ*dsyl*
Elongation	1.35 ± 0.03 (11)	1.27 ± 0.07 (11)	0.92 ± 0.19 (10)	1.28 ± 0.05 (16)
Shrinking	1.13 ± 0.07 (14)	1.02 ± 0.04 (11)	0.99 ± 0.03 (13)	1.33 ± 0.17 (21)
Frequencies (events/s)				
Catastrophe	0.0045 (13)	0.0023 (10)	0.0012 (12)*	0.0047 (20)
Rescue	0.0024 (9)	0.0019 (11)	0.0015 (10)*	0.0033 (16)
Event durations (min)				
Elongation	0.28 ± 0.03 (11)	0.30 ± 0.06 (11)	0.28 ± 0.09 (10)	0.26 ± 0.08 (16)
Shrinking	0.37 ± 0.01 (14)	0.31 ± 0.05 (11)	0.31 ± 0.10 (13)	0.33 ± 0.01 (21)
Pausing	0.54 ± 0.09 (26)	0.58 ± 0.09 (22)	1.48 ± 0.17 (21)*	0.45 ± 0.09 (35)

The dynamics of GFP-Tub1–labeled astral microtubules terminating in the bud (t = 0) were analyzed in small-budded cells (stacks acquired at 10-s intervals over a 310-s time lapse; see *Materials and Methods*). Event rates and durations are averaged values derived from triplicate analysis, ± SE. Values in parentheses are the number of events.

* Indicates significance at $p < 0.05$.

0.01) relative to *TUB4* (1.35 ± 0.03 μm·min^{-1}, $p < 0.01$), *kar9*Δ (1.27 ± 0.07 μm·min^{-1}, $p < 0.01$) and *tub4-*Δ*dsyl kar9*Δ cells (1.27 ± 0.05 μm·min^{-1}, $p < 0.01$), whereas the shrinkage rate of *tub4-*Δ*dsyl* cells was similar to that of the wild-type strain (Table 1). The frequency of catastrophes and rescues (events/s; Table 1) were also found to be decreased in *tub4-*Δ*dsyl* cells (0.0012 and 0.0015, $p < 0.05$) relative to *TUB4* (0.0045 and 0.0024; $p < 0.05$) and *tub4-*Δ*dsyl kar9*Δ cells (0.0047 and 0.0033; $p < 0.05$). Finally, although the average durations of elongation and shrinkage events in *tub4-*Δ*dsyl* cells were similar to those in *TUB4* cells, the time a microtubule spent in a paused state was greatly increased in *tub4-*Δ*dsyl* cells (88.6 ± 10.4 s; $p < 0.01$) relative to *TUB4* (32.4 ± 5.3 s), *kar9*Δ (35.0 ± 5.3 s), and *tub4-*Δ*dsyl kar9*Δ cells (27.2 ± 5.3 s) (Table 1). The increase in the duration of pauses and decrease in the frequency of catastrophe and rescue events in *tub4-*Δ*dsyl* cells correlated with an overall increase in net microtubule length throughout the time lapse (Figure 5). This analysis suggested that the altered dynamics of astral microtubules observed in *tub4-*Δ*dsyl* cells is unlikely to be the result of an alteration of

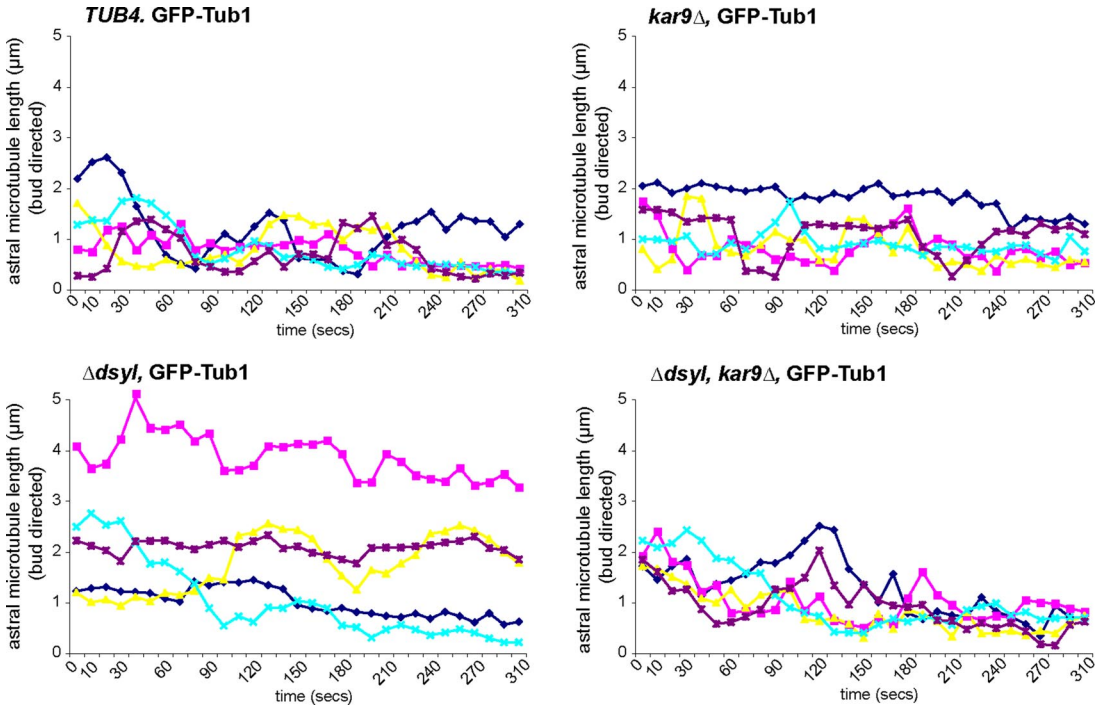

Figure 5. Preferential localization of Kar9 on microtubule +ends in *tub4-*Δ*dsyl* cells alters astral microtubule dynamics. Microtubule lifetime lengths were measured in *TUB4*, *tub4-*Δ*dsyl*, *kar9*Δ, and *tub4-*Δ*dsyl kar9*Δ cells containing a GFP–Tub1 fusion protein (see *Materials and Methods* for experimental details). Microtubule lengths (micrometers) were measured in triplicate at 10-s intervals (total time 310 s), and the averaged length was plotted relative to time (seconds). Astral microtubules in *tub4-*Δ*dsyl* cells were less dynamic relative to *TUB4* and *kar9*Δ cells with an increase in the duration of pause event. Dynamics are restored in *tub4-*Δ*dsyl kar9*Δ double mutant cells.

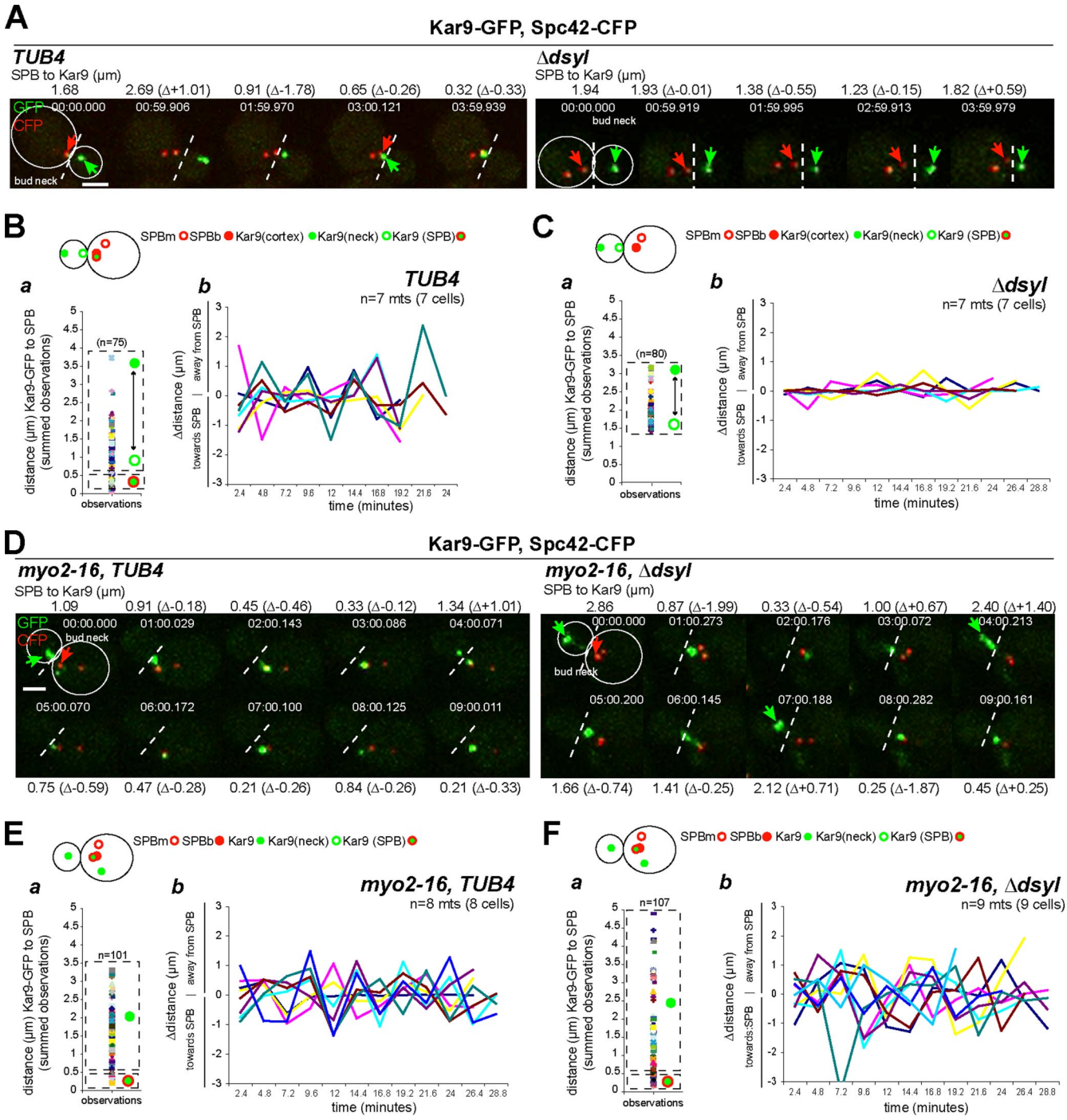

Figure 6. Kar9 interactions with Myo2 are stabilized in *tub4-Δdsyl* cells. (A) In *TUB4* cells microtubules loaded with Kar9 (green arrows) are dynamic and retract quickly from the cortex. In *tub4-Δdsyl* cells, Kar9-associated microtubules are less dynamic and rarely depolymerize back to the SPB_b (red arrows) or bud neck (indicated by dashed line). Mother and bud are outlined (white) in the first frame of the montage. (B) In wild-type cells, Kar9–GFP foci distribute near and far from the SPB_b (B, a). Kar9–GFP foci are highly dynamic and are associated with both growing and shrinking microtubules (B, b). In *tub4-Δdsyl* cells (C, a), the Kar9–GFP foci to not cluster near the SPB_b but rather to a region ~1.5–3 μm in length from the SPB_b. Furthermore, Kar9–GFP foci are not dynamic and are associated with microtubules that do not move toward and away from the SPB_b (C, b). (D) Montage ($t < 30$ min) of Kar9 foci in *myo2-16* cells and *tub4-Δdsyl myo2-16* double mutants revealed that Kar9 is dynamic in both cell types. Dashed line indicates bud neck. Bar, 2 μm. (E) In *myo2-16* Kar9–GFP foci have a large distribution due to the growth and shrinkage of dynamic microtubules (E, a). Microtubules in the *myo2-16* cells are dynamic due to short interactions with the cortex (E, b). (F) In *myo2-16*, *tub4-Δdsyl* double mutants, Kar9–GFP foci are distributed near the SPB_b and the bud cortex (F, a), whereas Kar9 dynamics are restored (F, b).

microtubule structure. In addition, this analysis suggested that in *tub4-Δdsyl* cells, Kar9 suppresses astral microtubule elongation and the frequency of catastrophe and rescue and increases the time microtubules spend in a paused state.

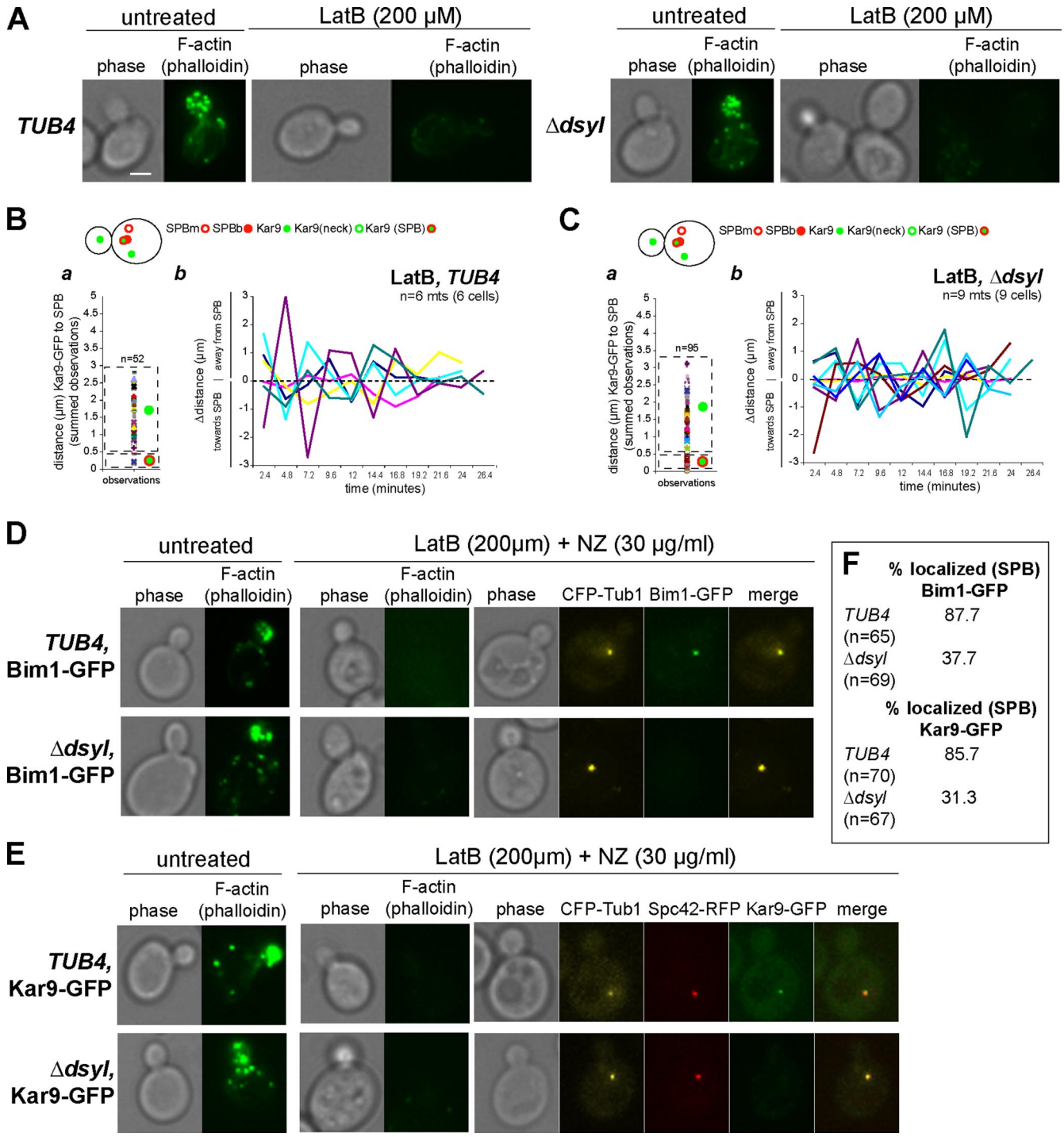

Figure 7. Stable localization of Kar9 in the bud depends on cortical actin. (A) Actin staining of *TUB4* and *tub4-Δdsyl* cells with and without treatment of 200 μM LatB. Treatment with LatB resulted in the depolymerization of the actin cytoskeleton in *TUB4* and *tub4-Δdsyl* cells. Respective phase images are shown. Bar, 2 μm. (B, a) In wild-type cells treated with LatB, Kar9–GFP foci distributed to at the bud cortex as well as the SPB. After latrunculin treatment, microtubules (Kar9–GFP foci) in wild-type cells were highly dynamic. In *tub4-Δdsyl* cells treated with latrunculin, the distribution of Kar9–GFP foci relative to the SPB were rescued to near wild-type levels (C, a). Kar9 dynamics were also rescued to near wild-type levels (C, b). (D–F) Analysis of Bim1 and Kar9 SPB localization in cells treated with 200 μM LatB (to disrupt F-actin) and 30 μg/ml NZ (to depolymerize astral microtubules). CFP–Tub1 was used to visualize the collapsed spindle and Alexa 488-phallodin to confirm the disruption of the actin cytoskeleton in the presence or absence of latrunculin and NZ. The majority of wild-type cells (87.7%; n = 65) treated with LatB and NZ had detectable Bim1–GFP associated with the collapsed spindle (D and F). In contrast, the percentage of LatB and NZ treated *tub4-Δdsyl* cells with detectable Bim1–GFP at SPBs was reduced (37.7%; n = 69) (D and F). Similarly, the localization of Kar9–GFP in *tub4-Δdsyl* cells treated with LatB and NZ was reduced; 31.3% of *tub4-Δdsyl* cells (n = 67) had detectable Kar9–GFP compared with 78% of wild-type cells (n = 70; E and F).

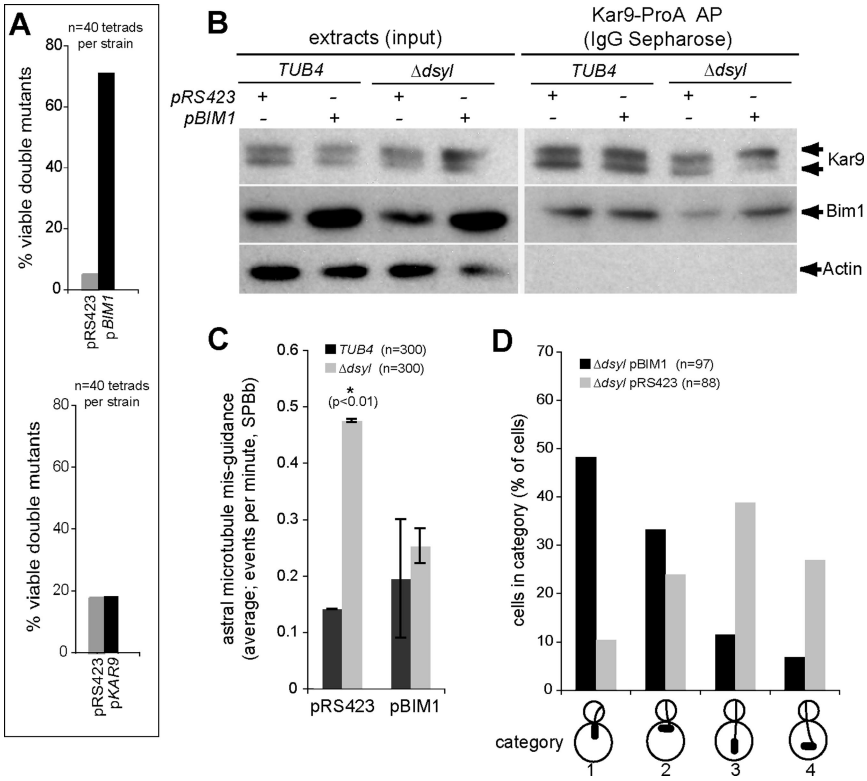

Figure 8. Kar9 function is restored by overproduction of Bim1. (A) Percentage of viable *tub4-Δdsyl Δdhc1* double mutants recovered in the presence of overproduced Bim1, Kar9 or vector control. Overproduction of Bim1 (*pBIM1*) rescued the synthetic lethality observed in *tub4-ΔdsylΔdhc1* double mutants, whereas overproduction of Kar9 (*pKAR9*) or expression of the vector control (*pRS423*) did not rescue synthetic lethality. Forty tetrads/mating were scored. (B) Bim1 and Kar9 interactions are restored by overproduction of Bim1. The level of Bim1 that coaffinity purifies with Kar9 in *tub4-Δdsyl* cells is restored in the presence of overproduced Bim1 relative to cells containing the vector control. (C) Astral microtubule guidance is restored by an overproduction of Bim1. *tub4-Δdsyl pBIM1* cells have a lower occurrence of microtubule misguidance relative to *tub4-Δdsyl pRS423* cells. (D) Spindle placement was analyzed in *tub4-Δdsyl pRS423* and *tub4-Δdsyl pBIM1* cells. Overproduction of Bim1 (black bars) rescued spindle positioning defects observed in control cells (gray bars).

Kar9 Interactions with Myo2 Are Stabilized in tub4-Δdsyl Cells

During spindle placement, Kar9 loaded microtubules probe the bud neck and cortex and then retract back to the SPB (Kusch *et al*., 2002; Liakopoulos *et al*., 2003; Maekawa *et al*., 2003). Consistent with this process, in wild-type cells, Kar9–GFP foci were found to probe the bud neck (dashed line) and retract to the SPB (Figure 6A and Supplemental Movie wt_supmov1.mov). During probing movements the spindle remained close to the bud neck (Figure 6A; distances in micrometers are shown above each frame of A). However, in *tub4-Δdsyl* cells, we observed Kar9–GFP dwelled either at the cortex or at the bud neck, and it rarely retracted back to the SPB (Figure 6A and Supplemental Movie dsyl_supmov2.mov). A summary of our analysis of the distribution of Kar9–GFP localization and movements in the bud, relative to the SPB (located in the mother cell or at the bud neck), for each strain/condition are shown in Figure 6, B and C (*TUB4*, n = 7 cells; *tub4-Δdsyl*, n = 7 cells). In wild-type cells, Kar9–GFP foci were distributed from the SPB_b and the bud neck, to the bud cortex (Figure 6B, a). Kar9–GFP movements in the bud in wild-type cells consisted of periodic movements away from and toward the SPB (Figure 6B, b). In contrast, the distribution of Kar9–GFP foci in *tub4-Δdsyl* cells was restricted to the bud, between the neck and the bud tip, and >1.0 μm from the SPB_b (Figure 6C, a). Consistently, the movement of Kar9–GFP foci in the bud was less dynamic in *tub4-Δdsyl* cells, with relatively few major (>0.5 μm) movements relative to the position of the SPB (Figure 6C, b).

Kar9 interacts with cortical actin via its association with the tail domain of the type V myosin Myo2, which guides microtubules loaded with Kar9 along polarized actin filaments during spindle positioning (Beach *et al*., 2000; Yin *et al*., 2000; Hwang *et al*., 2003). We speculated that the static localization of Kar9 in the bud and defect in Kar9 function was due to an inappropriately stable interaction between Kar9 and Myo2. To test this possibility, we analyzed Kar9–GFP movements in the *myo2-16* mutant, which is defective for Myo2-Kar9 interaction at 30°C in rich medium (Schott *et al*., 1999). Kar9–GFP movements were extremely dynamic in *myo2-16* cells; however, microtubules frequently failed to enter the bud, and spindle positioning was defective (Figure 6D). Next, we tested whether the *myo2-16* mutation would increase Kar9–GFP dynamicity in *tub4-Δdsyl* cells and eliminate cortical dwelling. Our analysis revealed that Kar9–GFP movements in *tub4-Δdsyl* cells were highly dynamic, although as in *myo2-16* cells, microtubule +end targeting into the bud and spindle positioning remained defective (Figure 6D). Kar9–GFP localization in the bud relative to the SPB and movements were monitored for each condition (*TUB4 myo2-16*, n = 8; *tub4-Δdsyl myo2-16*, n = 9; Figure 6, E and F). In *TUB4 myo2-16* cells, Kar9–GFP was detected at the bud neck, bud cortex, and SPB_b (Figure 6E, a). Kar9–GFP movements in the bud were highly dynamic, characterized by movements away from and toward the SPB (Figure 6E, b). Similarly, Kar9–GFP localized to the bud neck, bud cortex, and SPB_b in *myo2-16 tub4-Δdsyl* cells (Figure 6F, a). Moreover, Kar9–GFP movements in the bud were highly dynamic (Figure 6F, b). Together, these data suggests that the stable interaction between Kar9 and the cortex in *tub4-Δdsyl* cells is a result of inappropriately stable interactions between Kar9 and Myo2 and is consistent with the microtubule dynamics observed in *tub4-Δdsyl kar9Δ* double mutants.

Kar9 Dwelling in the Bud Requires Cortical Actin

We next wanted to confirm that the stable interaction between Kar9 and Myo2 was dependent on cortical actin, and we asked whether disruption of cortical F-actin structures by latrunculin B would restore dynamic Kar9–GFP movements in *tub4-Δdsyl* cells. Wild-type and *tub4-Δdsyl* cells expressing

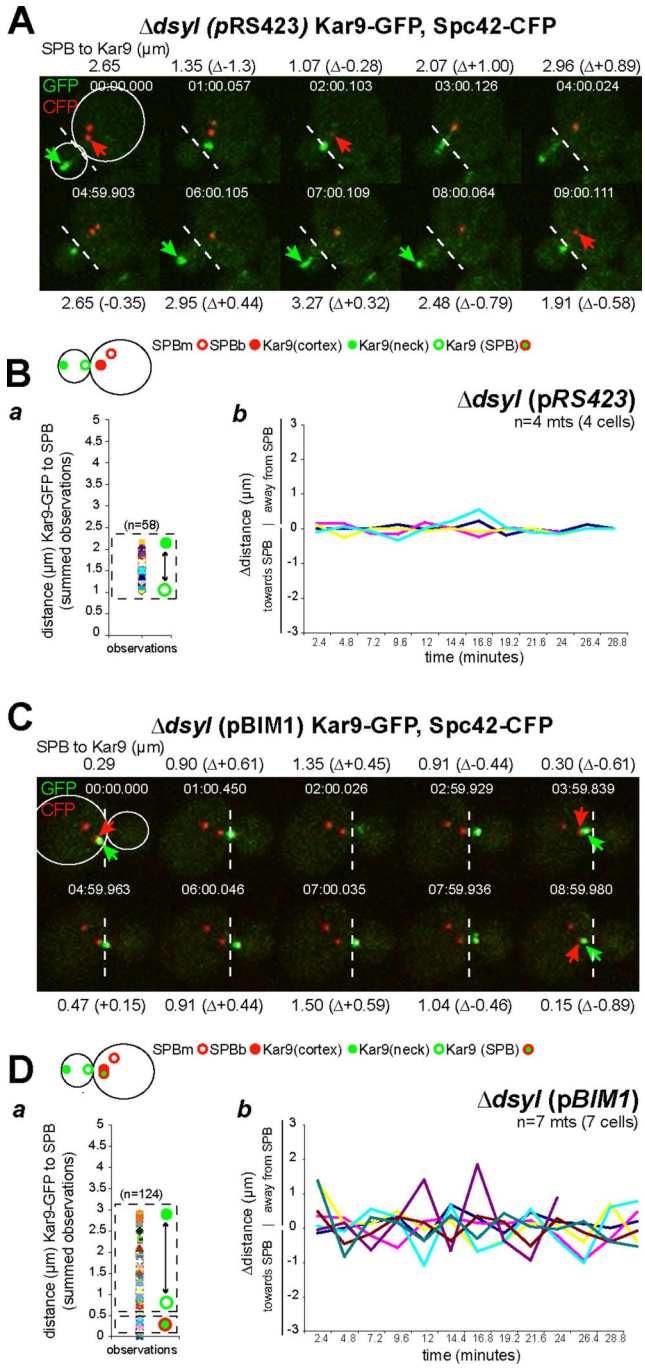

Figure 9. Overproduction of Bim1 restores Kar9 dynamics in *tub4-Δdsyl* cells. (A) Montage of Kar9–GFP movements in *tub4-Δdsyl pRS423* and *tub4-Δdsyl pBIM1* cells. Overproduction of Bim1 rescues the Kar9 associated microtubules dynamics in *tub4-Δdsyl* cells, whereas in the vector control, Kar9-associated microtubules remain un-dynamic (green arrows). (B and C) Microtubules/Kar9–GFP foci were tracked during a time course ($t < 30$ min) in *tub4-Δdsyl pRS423* and *tub4-Δdsyl pBIM1* cells. Line graphs depict the length from the microtubule +ends relative to the SPB_b per Δtime ($t = 2.4$ min). Scatter plots display the relative distribution of Kar9–GFP foci relative to the SPB over time. In *tub4-Δdsyl pRS423* cells (B, a), the Kar9–GFP foci cluster to a region ~1.5–3 μm in length from the SPB_b, indicating the microtubules do not depolymerize back to the SPB_b. Microtubules seemed to be static (B, b). In contrast, in *tub4-Δdsyl* cells with overproduced Bim1, the distribution of Kar9–GFP foci relative to the SPB_b (C, a) and its dynamic movement in the bud (C, b) were similar to wild type.

Kar9–GFP and Spc42–CFP were treated with 200 mM LatB for 30–60 min. Cells were stained with Alexa 488-phalloidin to confirm that F-actin was similarly disrupted in both strains (Figure 7A). Kar9–GFP localization was distributed between the cortex and SPB_b in wild-type cells treated with LatB (Figure 7B, a) characterized by highly dynamic movements between the SPB_b and bud cortex (Figure 7B, b). Similarly, *tub4-Δdsyl* cells also exhibited a distribution of Kar9–GFP foci between the SPB_b and cortex (Figure 7C, a) and dynamic movements within the bud (Figure 7C, b).

We next asked whether the dynamic movements of Kar9 in *tub4-Δdsyl* cells treated with LatB correlated with restoration of the microtubule-independent localization of Bim1 and/or Kar9 at SPBs. We reasoned that if the defect in SPB localization of these proteins is due to the loss of the DSYL residues, then releasing Kar9-complexes from cortex would not be expected to restore SPB localization of Bim1 or Kar9. To test this hypothesis, we analyzed the SPB localization of Bim1–GFP in wild-type and *tub4-Δdsyl* cells treated with LatB to disrupt F-actin, and NZ to depolymerize astral microtubules. CFP–Tub1 was used to visualize the collapsed spindle and Alexa 488-phallodin to confirm the disruption of the actin cytoskeleton. As before, we found the majority of wild-type cells (87.7%; n = 65) treated with LatB and NZ had detectable Bim1–GFP associated with the collapsed spindle (Figure 7, D and F). In contrast relatively few *tub4-Δdsyl* cells treated with LatB and NZ (37.7%; n = 69) had had detectable Bim1–GFP (Figure 7, D and F). Similarly, the localization of Kar9–GFP in *tub4-Δdsyl* cells treated with LatB and NZ was reduced; 31.3% of tub4-Δdsyl cells (n = 67) had detectable Kar9–GFP compared with 78% of wild-type cells (n = 70; Figure 7, E and F). This analysis suggests that the defect in Bim1 and Kar9 localization at SPBs in *tub4-Δdsyl* cells is independent of the interaction between Kar9 and the cortex.

Overproduction of Bim1 Restores Kar9 Function and Spindle Placement in tub4-Δdsyl Cells

Although Kar9 can localize to astral microtubules in *tub4-Δdsyl* cells, our analysis demonstrates that its localization is not sufficient for its function. We hypothesized that the ratio of Bim1 and Kar9 is critical for the assembly of functional Bim1–Kar9 complexes. As a consequence, the overproduction of Bim1 might restore Kar9–Bim1 interactions and rescue Kar9 function in *tub4-Δdsyl* cells, whereas overproduction of Kar9 would not. We first assayed for rescue of the Kar9 pathway by determining whether overproduction of either protein would restore viability to the *tub4-Δdsyl dhc1Δ* double mutant (Figure 2, B and C). *tub4-Δdsyl* cells were transformed with a 2μ vector (pRS423) containing *BIM1* or *KAR9* or 2μ vector and mated to *dhc1Δ* cells to produce heterozygous diploid strains. Haploid progeny (40 tetrads/condition) were scored for the presence of viable double mutants. We found overproduction of Bim1 increased the viability *tub4-Δdsyl dhc1Δ* double mutants (Figure 8A). However, overproduction of Kar9 did not increase viability, nor did the vector control (Figure 8A).

We next assessed whether overproduction of Bim1 would increase the amount of Bim1 copurifying with Kar9–ProA in *tub4-Δdsyl* cells. Kar9–ProA was affinity purified from whole cell extracts prepared from wild-type and *tub4-Δdsyl* cells overproducing Bim1 (p*BIM1*) or endogenous Bim1 (pRS423). Bim1 levels increased in *tub4-Δdsyl* cells containing pBIM1, and the amount of Bim1 copurifying with Kar9–ProA was restored to wild-type levels (Figure 8B). As before, *tub4-Δdsyl* cells expressing endogenous levels of Bim1 had reduced Bim1 copurifying with Kar9–ProA (Figure 8B).

We next tested whether overproduction of Bim1 would rescue the defect in microtubule targeting and spindle placement observed in *tub4-Δdsyl* cells. This analysis revealed overproduction of Bim1 suppressed mistargeting in *tub4-Δdsyl* cells relative to the vector control (Figure 8C). Similarly, defects in spindle placement were rescued in *tub4-Δdsyl* cells overproducing Bim1 relative to the control (Figure 8D). Collectively, these analyses suggested that overproduction of Bim1 can restore its interaction with Kar9 in *tub4-Δdsyl* cells.

We then asked whether overproduction of Bim1 in *tub4-Δdsyl* cells would reduce the cortical dwelling of Kar9–GFP in the bud, and we analyzed the distribution and movements of Kar9–GFP in the bud relative to the position of the SPB_b over time in *tub4-Δdsyl pRS423* and *tub4-Δdsyl pBIM1* cells. In *tub4-Δdsyl pRS423* cells, Kar9–GFP movements in the bud did not pull the spindle toward the neck or orient it; at 3 min, the spindle rotates and becomes misoriented and remains misoriented and positioned away from the bud neck for the remainder of the time lapse (Figure 9A and Supplemental Movie p423_supmov3.mov). In contrast, Kar9–GFP movements were more dynamic and associated with astral microtubules that probed the neck/cortex and retracted back to the SPB_b in *tub4-Δdsyl* cells overproducing Bim1 (Figure 9C and Supplemental Movie pBIM1_supmov4.mov).

A summary of our analysis of Kar9–GFP movements in representative cells for each strain and condition (*tub4-Δdsyl* pRS423, n = 4; *tub4-Δdsyl* p*BIM1*, n = 7) is shown in Figure 9, B and D. In *tub4-Δdsyl pRS423* cells, Kar9–GFP was detected at the cortex and bud neck but not at the SPB (Figure 9B, a) and dwelled in these locations without dynamic movement (Figure 9B, b). However, overproduction of Bim1 in *tub4-Δdsyl* cells restored SPB localization of Kar9–GFP (Figure 9D, a) and its dynamic movement in the bud (Figure 9D, b). Together, our analysis suggests that overproduction of Bim1 in *tub4-Δdsyl* cells promotes the assembly of functional Bim1–Kar9 complexes.

DISCUSSION

Roles of Tub4 and SPBs in Kar9-dependent Spindle Positioning

Numerous studies have demonstrated that the SPBs play a critical role in Kar9-dependent spindle positioning. For example, the asymmetric localization of Kar9 to the SPB_b ensures its deployment to the astral microtubules adjacent to the bud, which is essential for its function in spindle positioning (Liakopoulos *et al*., 2003; Maekawa *et al*., 2003; Maekawa and Schiebel, 2004; Moore *et al*., 2006). Phospho-inhibiting mutations in residues Ser197 and S496 (*kar9-AA*), block phosphorylation by Cdk1/Clb4, and result in the symmetric localization of Kar9 to both SPBs, inappropriate targeting of astral microtubules associated with both SPBs to the bud, and an increase in the number of cells with misoriented spindles positioned near the bud neck (Liakopoulos *et al*., 2003). Conversely, loss of Kar9 function (by deletion of Kar9 or genes acting in the Kar9 pathway), results in mistargeting of microtubules emanating from the SPB_b back into the mother cell and failure to orient the spindle (Miller and Rose, 1998; Liakopoulos *et al*., 2003). In *tub4-Δdsyl* cells, Kar9 remains associated with microtubules emanating from the SPB_b and misoriented spindles positioned at the bud neck are rarely observed, indicating its asymmetric localization to astral microtubules is preserved. Although *tub4-Δdsyl* cells are less efficient in targeting astral microtubules into the bud, astral microtubules loaded with Kar9 frequently enter the bud but fail to place the spindle at the bud neck. The observed defect in spindle placement in *tub4-Δdsyl* cells is therefore not characteristic of a defect in establishing asymmetry, or a loss of function *kar9Δ* mutation. Instead, the defect in spindle positioning observed in *tub4-Δdsyl* cells seems to be linked to the ability of Kar9-complexes to function on microtubule +ends rather than to localize to +ends. Our analysis suggests that the SPB, via the C terminus of Tub4, contributes to the loading and/or assembly of functional Bim1–Kar9 complexes before their deployment to astral microtubules.

Dynamic Interactions between Kar9 and the Cortex Start at the SPB

The cortical dwelling observed in *tub4-Δdsyl* cells suggests defective +TIP complexes containing Kar9 can tether the +ends of astral microtubules to the cortex of the bud tip, suppressing microtubule dynamics and perturbing the function of the Kar9 pathway. Our analysis suggests that components of the Bim1–Kar9 complex that regulate its interaction with the cortex are loaded at the SPB and that this loading is dependent on Tub4. In *tub4-Δdsyl* cells, we observed astral microtubules undergo long pauses and have a slower rate of elongation than astral microtubules in wild-type cells. Significantly, deletion of Kar9 in the *tub4-Δdsyl* mutant increased the elongation rate and decreased the time astral microtubules spent in a paused state. This result strongly suggests that a defective Kar9-complex suppresses the dynamics of astral microtubules in the bud in *tub4-Δdsyl* cells. We also observed a significant increase in the amount of Kar9–GFP associated with the +ends of astral microtubules in the bud, which could be the result of an inappropriately stable interaction with Myo2 and/or cortical actin structures located at the tip of the bud. Based on our results, we conclude that the release of microtubules loaded with Kar9 from the cortex is defective in *tub4-Δdsyl* cells.

We propose that the initial loading of Bim1 and Kar9 at the SPB plays a critical role in assembling a functional +TIP complex, and thus effects how microtubules loaded with Kar9 complexes will subsequently interact with the cortex. It is likely that other proteins that localize to microtubule +ends, or to the bud tip, participate in this process. For example, a kinesin such as Kip3, which travels with Kar9 to the +end, or the −end-directed motor Kar3, may facilitate the release of Kar9 from Myo2 at the bud tip (Meluh and Rose, 1990; Endow *et al*., 1994; Miller *et al*., 1998; Liakopoulos *et al*., 2003). Alternately, a negative regulator of the Kar9–Myo2 interaction may travel with Kar9 to the cortex in an inactive state and be activated when the Kar9–Myo2 complex reaches polarity proteins located in the tip of the bud. These possibilities are not mutually exclusive and could act in combination to coordinate depolymerization of the +end with release of Kar9 from Myo2 at the bud tip.

Bim1–Kar9 Interactions at the Cortex

Recent studies indicate that the stoichiometry of APC and EB1, +TIP proteins that share homology with Kar9 and Bim1 respectively, have functional consequences on microtubule dynamics and organization (Nakamura *et al*., 2001; Green *et al*., 2005). Additionally, previous studies suggest that frequency of pauses increases in cells lacking Bim1, resulting in shorter astral microtubules (Tirnauer *et al*., 1999). It is therefore reasonable to conclude that a decreased ratio of Bim1 and Kar9 at astral microtubule +ends would similarly alter microtubules dynamics. Although the time astral microtubule spent paused is similarly increased in *tub4-Δdsyl* cells, long astral microtubules are observed rather than short microtubules. We suggest that Kar9, which does not associate with microtubules in the absence of Bim1, is responsible for this difference; Bim1 levels

are reduced but Kar9 remains associated with the microtubule, with Myo2, and with cortical actin. This is consistent with a previous study that suggests Kar9, via polarity proteins such as Bud6, may promote microtubule stabilization within the bud (Huisman *et al*., 2004). We speculate that the decreased Bim1–GFP signal at microtubule +ends may be result of its disassociation from Kar9 when the complex dwells at the cortex.

Tub4 as a Scaffold: A Model for Postnucleation Function in Microtubule Organization

The defects in Bim1 and Kar9 SPB localization observed in *tub4-Δdsyl* cells correlates with perturbation of the function of the Kar9 pathway, suggesting that the initial localization of +TIP proteins to SPBs is important for both establishing asymmetry and for assembling a functional Bim1–Kar9 complex. We propose that Tub4, via its carboxy terminus, may influence the function of proteins involved in the loading and/or deployment of Bim1 and Kar9 at SPBs. Tub4 does not seem to directly interact with Bim1 or Kar9 based on copurification experiments (our unpublished data), and the incomplete penetrance of the defect in SPB loading further suggests that this aspect of Tub4 function is mediated through its interaction with an as yet unidentified effector protein or complex. However, Bim1's ability to load at the SPB is likely to be important for complex formation. Overproduction of Bim1 in *tub4-dsyl* cells may stabilize its interaction with Kar9 at SPBs and allow a functional Kar9 complex to assemble before its deployment to the microtubule. We cannot exclude the possibility that overproduction of Bim1 also promotes its association with Kar9 at +ends and thereby restores normal interactions between the +TIP complex and the cortex of the bud.

Our analysis supports a novel postnucleation role for Tub4 in influencing the behavior of astral microtubules through +TIP proteins. The effect of the *tub4-Δdsyl* mutation on microtubule dynamics is rescued by deletion of Kar9, strongly suggesting that Tub4 influences microtubule dynamics through +TIPs instead of altering the structure of the microtubule lattice as proposed previously (Usui and Schiebel, 2001). An exciting possibility is that the highly accessible c-terminus of γ-tubulin (Aldaz *et al*., 2005) acts as a scaffold at the interface between the SPB and the −ends of microtubules. This possible role for Tub4 may spark a renewed interest in previous studies implicating γ-tubulin in nucleation-independent aspects of microtubule organization (Masuda and Shibata, 1996; Paluh *et al*., 2000; Vogel and Snyder, 2000; Vogel *et al*., 2001).

ACKNOWLEDGMENTS

We thank Howard Bussey, Guillaume Lesage (Cell Imaging and Analysis Network, McGill University), Craig Mandato, and Monique Zetka for critical reading of the manuscript. We thank Robin Battye, Jelena Jevtic, and John Arbuckle (Quorum Technologies) for ongoing support and development of the WaveFX imaging system. J.V. is supported by New Investigator Award MSH 69117 from the Canadian Institutes of Health Research. R.M. is supported by Grant MCB 0414768 from the National Science Foundation. This research was supported by operating Grant MOP-64404 from the Canadian Institutes of Health Research and infrastructure Grants CFI 7395 from the Canada Foundation for Innovation to J.V. and to the Developmental Biology Research Initiative of McGill University (CFI 8298).

REFERENCES

Adames, N. R., and Cooper, J. A. (2000). Microtubule interactions with the cell cortex causing nuclear movements in *Saccharomyces cerevisiae*. J. Cell Biol. *149*, 863–874.

Aldaz, H., Rice, L. M., Stearns, T., and Agard, D. A. (2005). Insights into microtubule nucleation from the crystal structure of human γ-tubulin. Nature *435*, 523–527.

Beach, D. L., Thibodeaux, J., Maddox, P., Yeh, E., and Bloom, K. (2000). The role of the proteins Kar9 and Myo2 in orienting the mitotic spindle of budding yeast. Curr. Biol. *10*, 1497–1506.

Carminati, J. L., and Stearns, T. (1997). Microtubules orient the mitotic spindle in yeast through dynein-dependent interactions with the cell cortex. J. Cell Biol. *138*, 629–641.

Christianson, T. W., Sikorski, R. S., Dante, M., Shero, J. H., and Hieter, P. (1992). Multifunctional yeast high-copy-number shuttle vectors. Gene *110*, 119–122.

Endow, S. A., Kang, S. J., Satterwhite, L. L., Rose, M. D., Skeen, V. P., and Salmon, E. D. (1994). Yeast Kar3 is a minus-end microtubule motor protein that destabilizes microtubules preferentially at the minus ends. EMBO J. *13*, 2708–2713.

Green, R. A., Wollman, R., and Kaplan, K. B. (2005). APC and EB1 function together in mitosis to regulate spindle dynamics and chromosome alignment. Mol. Biol. Cell *16*, 4609–4622.

Guthrie, C., and Fink, G. R. (1991). Guide to Yeast Genetics and Molecular Biology Part B, New York: Academic Press.

Huisman, S. M., Bales, O. A., Bertrand, M., Smeets, M. F., Reed, S. I., and Segal, M. (2004). Differential contribution of Bud6p and Kar9p to microtubule capture and spindle orientation in *S. cerevisiae*. J. Cell Biol. *167*, 231–244.

Hwang, E., Kusch, J., Barral, Y., and Huffaker, T. C. (2003). Spindle orientation in *Saccharomyces cerevisiae* depends on the transport of microtubule ends along polarized actin cables. J. Cell Biol. *161*, 483–488.

Kosco, K. A., Pearson, C. G., Maddox, P. S., Wang, P. J., Adams, I. R., Salmon, E. D., Bloom, K., and Huffaker, T. C. (2001). Control of microtubule dynamics by Stu2p is essential for spindle orientation and metaphase chromosome alignment in yeast. Mol. Biol. Cell *12*, 2870–2880.

Kusch, J., Meyer, A., Snyder, M. P., and Barral, Y. (2002). Microtubule capture by the cleavage apparatus is required for proper spindle positioning in yeast. Genes Dev. *16*, 1627–1639.

Lee, L., Tirnauer, J. S., Li, J., Schuyler, S. C., Liu, J. Y., and Pellman, D. (2000). Positioning of the mitotic spindle by a cortical-microtubule capture mechanism. Science *287*, 2260–2262.

Liakopoulos, D., Kusch, J., Grava, S., Vogel, J., and Barral, Y. (2003). Asymmetric loading of Kar9 onto spindle poles and microtubules ensures proper spindle alignment. Cell *112*, 561–574.

Longtine, M. S., McKenzie, A., 3rd, Demarini, D. J., Shah, N. G., Wach, A., Brachat, A., Philippsen, P., and Pringle, J. R. (1998). Additional modules for versatile and economical PCR-based gene deletion and modification in *Saccharomyces cerevisiae*. Yeast *14*, 953–961.

Louie, R. K., Bahmanyar, S., Siemers, K. A., Votin, V., Chang, P., Stearns, T., Nelson, W. J., and Barth, A. I. (2004). Adenomatous polyposis coli and EB1 localize in close proximity of the mother centriole and EB1 is a functional component of centrosomes. J. Cell Sci. *117*, 1117–1128.

Maekawa, H., and Schiebel, E. (2004). Cdk1-Clb4 controls the interaction of astral microtubule plus ends with subdomains of the daughter cell cortex. Genes Dev. *18*, 1709–1724.

Maekawa, H., Usui, T., Knop, M., and Schiebel, E. (2003). Yeast Cdk1 translocates to the plus end of cytoplasmic microtubules to regulate bud cortex interactions. EMBO J. *22*, 438–449.

Marschall, L. G., Jeng, R. L., Mulholland, J., and Stearns, T. (1996). Analysis of Tub4p, a yeast γ-tubulin-like protein: implications for microtubule-organizing center function. J. Cell Biol. *134*, 443–454.

Masuda, H., and Shibata, T. (1996). Role of γ-tubulin in mitosis-specific microtubule nucleation from the *Schizosaccharomyces pombe* spindle pole body. J. Cell Sci. *109*, 165–177.

Meluh, P. B., and Rose, M. D. (1990). KAR3, a kinesin-related gene required for yeast nuclear fusion. Cell *60*, 1029–1041.

Miller, R. K., Cheng, S. C., and Rose, M. D. (2000). Bim1p/Yeb1p mediates the Kar9p-dependent cortical attachment of cytoplasmic microtubules. Mol. Biol. Cell *11*, 2949–2959.

Miller, R. K., Heller, K. K., Frisen, L., Wallack, D. L., Loayza, D., Gammie, A. E., and Rose, M. D. (1998). The kinesin-related proteins, Kip2p and Kip3p, function differently in nuclear migration in yeast. Mol. Biol. Cell *9*, 2051–2068.

Miller, R. K., and Rose, M. D. (1998). Kar9p is a novel cortical protein required for cytoplasmic microtubule orientation in yeast. J. Cell Biol. *140*, 377–390.

Moore, J. K., D'Silva, S., and Miller, R. K. (2006). The CLIP-170 homologue Bik1p promotes the phosphorylation and asymmetric localization of Kar9p. Mol. Biol. Cell *17*, 178–191.

Nakamura, M., Zhou, X. Z., and Lu, K. P. (2001). Critical role for the EB1 and APC interaction in the regulation of microtubule polymerization. Curr. Biol. *11*, 1062–1067.

Paluh, J. L., Nogales, E., Oakley, B. R., McDonald, K., Pidoux, A. L., and Cande, W. Z. (2000). A mutation in γ-tubulin alters microtubule dynamics and organization and is synthetically lethal with the kinesin-like protein pkl1p. Mol. Biol. Cell *11*, 1225–1239.

Pereira, G., Tanaka, T. U., Nasmyth, K., and Schiebel, E. (2001). Modes of spindle pole body inheritance and segregation of the Bfa1p-Bub2p checkpoint protein complex. EMBO J. *20*, 6359–6370.

Pot, I., Knockleby, J., Aneliunas, V., Nguyen, T., Ah-Kye, S., Liszt, G., Snyder, M., Hieter, P., and Vogel, J. (2005). Spindle checkpoint maintenance requires Ame1 and Okp1. Cell Cycle *4*, 1448–1456.

Puig, O., Caspary, F., Rigaut, G., Rutz, B., Bouveret, E., Bragado-Nilsson, E., Wilm, M., and Seraphin, B. (2001). The tandem affinity purification (TAP) method: a general procedure of protein complex purification. Methods *24*, 218–229.

Schott, D., Ho, J., Pruyne, D., and Bretscher, A. (1999). The COOH-terminal domain of Myo2p, a yeast myosin V, has a direct role in secretory vesicle targeting. J. Cell Biol. *147*, 791–808.

Sobel, S. G., and Snyder, M. (1995). A highly divergent γ-tubulin gene is essential for cell growth and proper microtubule organization in *Saccharomyces cerevisiae*. J. Cell Biol. *131*, 1775–1788.

Spang, A., Geissler, S., Grein, K., and Schiebel, E. (1996). γ-Tubulin-like Tub4p of *Saccharomyces cerevisiae* is associated with the spindle pole body substructures that organize microtubules and is required for mitotic spindle formation. J. Cell Biol. *134*, 429–441.

Straight, A. F., Marshall, W. F., Sedat, J. W., and Murray, A. W. (1997). Mitosis in living budding yeast: anaphase A but no metaphase plate. Science *277*, 574–578.

Tirnauer, J. S., O'Toole, E., Berrueta, L., Bierer, B. E., and Pellman, D. (1999). Yeast Bim1p promotes the G1-specific dynamics of microtubules. J. Cell Biol. *145*, 993–1007.

Tong, A. H., *et al*. (2001). Systematic genetic analysis with ordered arrays of yeast deletion mutants. Science *294*, 2364–2368.

Usui, T., and Schiebel, E. (2001). Regulating microtubule properties by modifying their organizing minus ends. Mol. Cell *8*, 931–932.

Vogel, J., Drapkin, B., Oomen, J., Beach, D., Bloom, K., and Snyder, M. (2001). Phosphorylation of γ-tubulin regulates microtubule organization in budding yeast. Dev. Cell *1*, 621–631.

Vogel, J., and Snyder, M. (2000). The carboxy terminus of Tub4p is required for γ-tubulin function in budding yeast. J. Cell Sci. *113*, 3871–3882.

Yin, H., Pruyne, D., Huffaker, T. C., and Bretscher, A. (2000). Myosin V orientates the mitotic spindle in yeast. Nature *406*, 1013–1015.